Journal of Engineering Physics and Thermophysics, Vol. 74, No. 4, 2001

THERMAL GRAVITATIONAL-CAPILLARY CONVECTION IN A CAVITY WITH A LONGITUDINAL TEMPERATURE GRADIENT

V. S. Berdnikov, V. A. Gaponov, and L. S. Kovrizhnykh

UDC 536.24;532.529.2;621.746

Convective heat exchange in a flow of liquid in a rectangular cavity with the length-to-height ratio of a liquid layer L/H = 10 is investigated. The conditions of thermal insulation or linear distribution of temperature were kept on the lower horizontal surface. Three types of boundary conditions for velocity were set on the upper boundary: rigid, free without friction, and free with imposition of a thermocapillary effect. The vertical walls of the cavity are isothermal and heated to different temperatures. The investigated regimes were of thermogravitational, thermocapillary, and thermal gravitational-capillary convection. A comparative analysis of the evolution of flow structure with increase in the Rayleigh (Ra) and Marangoni (Ma) numbers is carried out.

We investigated, numerically and experimentally, convective heat exchange in viscous incompressible liquid flow in a long rectangular cavity $A = L/H = 10$ with isothermal vertical walls heated up to different temperatures. This thermohydrodynamic system can be considered as a simplified model of one of the methods of obtaining single crystals from melts, i.e., the method of horizontal directed crystallization [1, 2]. To create a controlled technology, it is important to know: (1) the laws governing the evolution of the spatial form of flow with increase in the longitudinal temperature gradient under different conditions on horizontal walls; (2) the degree of the effect of local particular features of the spatial form of flow on changes in the shape of isotherms and local thermal fluxes on a cold wall. These parameters characterize the shape of the crystallization front and thermal stresses in a crystal, which determines the perfection of its structure. The present work is a natural continuation of investigations into hydrodynamics and heat exchange [1–3] in plane layers and cavities with a longitudinal temperature gradient. The results presented below represent the next stage in goal-directed investigations [3, 4] of the relative contribution of gravitational and capillary forces in the formation of flow structure.

In the numerical simulation, three types of boundary conditions were prescribed on the upper boundary for the velocity: rigid, free without friction, and free with imposition of a thermocapillary effect. For the temperature, two conditions were assigned on the rigid upper wall: thermal insulation [3] and a linear distribution of temperature; the condition of thermal insulation is always fulfilled on the free (rectilinear and nondeformed) boundary. The lower rigid horizontal surface was adiabatic or a linear distribution of temperature was prescribed [3]. For a liquid with Prandtl number Pr = 16, the regime of thermogravitational convection was investigated with increase in Ra from 10 to 10^6 and that of thermocapillary convection with increase in the Marangoni number Ma from 10 to 10^4; in the entire range of Ra and Ma numbers, the regime of thermal gravitational-capillary convection was investigated. In the latter regime, the developed thermocapillary convection is taken as the initial state. Thereafter, the evolution of the flow structure with increase in the contribution of buoyancy forces is investigated for Ma = idem. Comparison of the local features of flow,

S. S. Kutateladze Institute of Thermophysics, Siberian Branch of the Russian Academy of Sciences, Novosibirsk, Russia; email: berdnikov@itp.nsc.ru. Translated from Inzhenerno-Fizicheskii Zhurnal, Vol. 74, No. 4, pp. 116–121, July–August, 2001. Original article submitted September 11, 2000.

temperature fields, and local and integral heat fluxes, attributable to heat conduction and convection, on the walls of the cavity and in different sections in the volume of the liquid, at different combinations of the relative contribution of buoyancy forces and thermocapillary effect, makes it possible to investigate the mechanisms of their nonlinear interaction and influence on the processes of heat exchange.

Computations were carried out by the method of compact differences [5, 6] on nonuniform grids with the fifth order of accuracy. The principle of separate solution of equations, time-dependent technique, and the method of fractional steps were used. Rectangular nonuniform grids, extending to the center and contracting to the boundaries of the region, of size 400 × 40 mesh with a minimum step of 0.008 over each of the space coordinates were used. As was shown in [7], for the case of a square cavity the increase in the order of the schemes used [6] leads not only to quantitative, but also to qualitative differences from the earlier obtained results on computational local characteristics [8].

The system of equations in the Boussinesq approximation is

$$\frac{\partial \omega}{\partial t} + \frac{\partial}{\partial x}(u\omega) + \frac{\partial}{\partial y}(v\omega) = \mathrm{Pr}\,\nabla^2\omega - \mathrm{Ra}\,\mathrm{Pr}\,\frac{\partial T}{\partial x}, \quad \nabla^2\psi = \omega,$$

$$\frac{\partial T}{\partial t} + \frac{\partial}{\partial x}(uT) + \frac{\partial}{\partial y}(vT) = \nabla^2 T, \quad u = \frac{\partial \psi}{\partial y}, \quad v = -\frac{\partial \psi}{\partial x}, \quad \omega = \frac{\partial u}{\partial y} - \frac{\partial v}{\partial x}.$$

The boundary conditions are

for $x = 0$: $\psi = \partial\psi/\partial x = 0,\ T = 0.5$;

for $x = A$: $\psi = \partial\psi/\partial x = 0,\ T = -0.5$;

for $y = 0$: 1) $\psi = \partial\psi/\partial y = 0,\ \partial T/\partial y = 0$; 2) $\psi = \partial\psi/\partial y = 0,\ T = 0.5 - x/A$;

for $y = 1$: 1) $\psi = \partial\psi/\partial y = 0,\ T = 0.5 - x/A$; 2) $\psi = \partial\psi/\partial y = 0,\ \partial T/\partial y = 0$; 3) $\psi = \partial^2\psi/\partial^2 y = 0,\ \partial T/\partial y = 0$; 4) $\psi = 0,\ \partial^2\psi/\partial^2 y = -\mathrm{Ma}\,\partial T/\partial x,\ \partial T/\partial y = 0$.

The quantities are made dimensionless (the dimensional quantities are primed) as

$$x = x'/H, \quad y = y'/H, \quad A = L/H; \quad \{u, v\} = \{u', v'\}\,H/a; \quad T = (T' - T_0)/\Delta T,$$

$$T_0 = (T_1 + T_2)/2, \quad \Delta T = T_1 - T_2 > 0.$$

Analysis of the evolution of the isolines of the stream function showed that the flow has a simple single-contour circulation in all the investigated ranges of the Ra and Ma numbers [3] for all of the combinations of boundary conditions. The typical pattern of evolution of the temperature field for all the regimes is: up to the threshold values of Ra and Ma that depend on the type of conditions on horizontal boundaries, the regime of heat conduction is preserved to which a plane-parallel flow in the region $1 \le x \le 9$ corresponds. For example, in the regime of thermocapillary convection up to Ma = 200, heat conduction remains the main mechanism of heat transfer. Here, up to Ma = 10 the isotherms are strictly vertical and the temperature profiles $T(y)$ coincide with them (Fig. 1a); temperature distributions along the longitudinal coordinate in different sections y (Fig. 1b) merge into a single straight line: $T(x) = T_1 - x/A$. At Ma = 100, the isotherms are only slightly deformed, i.e., they are "torn away" by the upper branch of the flow.

Figure 1 shows the distributions of temperature and velocity in different sections in the vertical direction (a, c) and in the horizontal one (b, d) at Ma = 1000 (the regime of thermocapillary convection, a linear distribution of temperature on the bottom). The velocity components are additionally normalized to the value $[\mathrm{Ra} + (\mathrm{Ma})^2]^{1/2}$. In this regime, the deformation of isotherms is substantial. Owing to the entrainment of the hot liquid to the free surface and of the cold one to the bottom, there is already a noticeable stratification of liquid by temperature. The most significant detail is the appearance of a small section of a boundary layer on

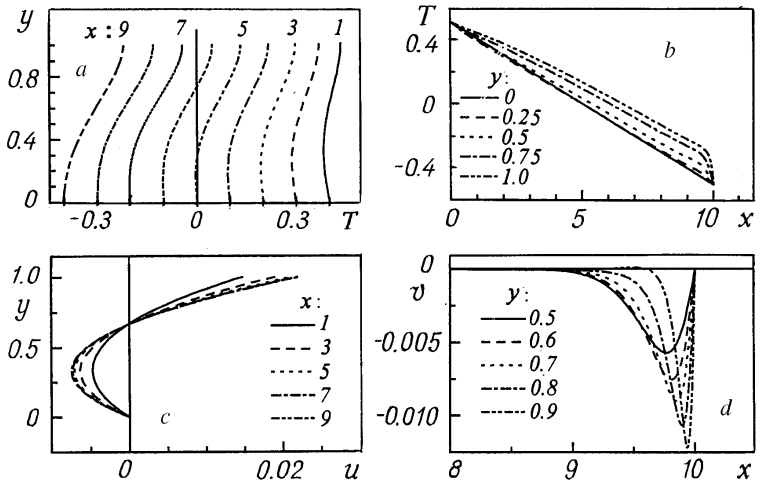

Fig. 1. Characteristics of the profiles of temperature and velocity fields in the regime of thermocapillary convection (Ma = 1000): a) $T(x_i, y)$; c) $u(x_i, y)$ in different sections $x = x_i$; b) $T(x, y_j)$; d) $v(x, y_j)$ in different sections $j = y_j$.

the lower boundary of the cavity where the curve $T(x; 1/4)$ intersects, and then goes below, the straight line $T(x; 0)$ showing the distribution of temperature on the lower wall, i.e., a section appears in the lower branch of the flow where there is an inflow of a relatively cold liquid onto the hotter and hotter wall. As Ma increases, the size of this section and the absolute value of the temperature gradient along the normal to the bottom increase, which resembles the appearance of the section of an unstably stratified boundary layer in the regime of thermogravitational convection [3]. These effects are observed when $\mathrm{Ma} \geq 200$.

The rearrangement of the temperature field is interconnected with the enhancement of convective motion and change in the velocity field with increase in Ma. For $\mathrm{Ma} \leq 500$ in the range $1 \leq x \leq 9$ the flow is virtually plane-parallel and the profiles of the longitudinal velocity component are independent of x. Qualitatively they coincide with the analytical solution for an infinite layer with a longitudinal temperature gradient [4] and experimentally measured profiles $u(y)$ in the central portion of the long layer [1, 2]. As Ma increases, the velocity profiles and the value of $u_{\max}$ become dependent on the longitudinal coordinate (Figs. 1c, 2b). The turning regions at the end faces of the cavity for $\mathrm{Ma} \leq 500$ have an extension equal approximately to the height of the layer (Fig. 1d). Figure 2 shows the evolution of longitudinal distributions of temperature (a) and of normalized velocity (b) on the free surface with increase in Ma. It is seen in which way the heat-conduction regime ($\mathrm{Ma} \leq 10$) passes to a constrained regime ($\mathrm{Ma} \geq 2000$), where a sharp burst of the longitudinal velocity component is observed near the cold wall. The asymmetry of the spatial form of the flow and of the temperature field, which is increased with Ma, is accompanied by violation of the symmetry in the distribution of a local heat flux on the end faces and on the lower horizontal surface similarly to the regime of thermal gravitational convection [3]. Figure 2 shows the distributions of local heat fluxes on hot (c) and cold (d) walls for different values of Ma. On the hot wall the heat transfer is determined by the incoming flow in the bottom region and on the cold wall by the sharp increase in heat transfer on the portion near the free surface. The thermocapillary flow is incident on the cold wall in the form of a compact jet of a hot liquid, and this explains the abnormally high values of the local heat flux $q(y)$ and its maximum value $q(1)$ in Fig. 2d. Downstream, along the cold wall in the region $0.9 \leq y \leq 1$, the value of $q(y)$ for Ma = 5000 drops by an order of magnitude. These features are also well seen from the character of the change in the family of isotherms near the cold wall. The dependences of the integral heat transfer (Fig. 3a) on rigid walls are obtained: Q_1 is the heat flux from the hot wall, Q_2 is the heat flux on the cold wall, Q_3 and Q_4 are the heat fluxes

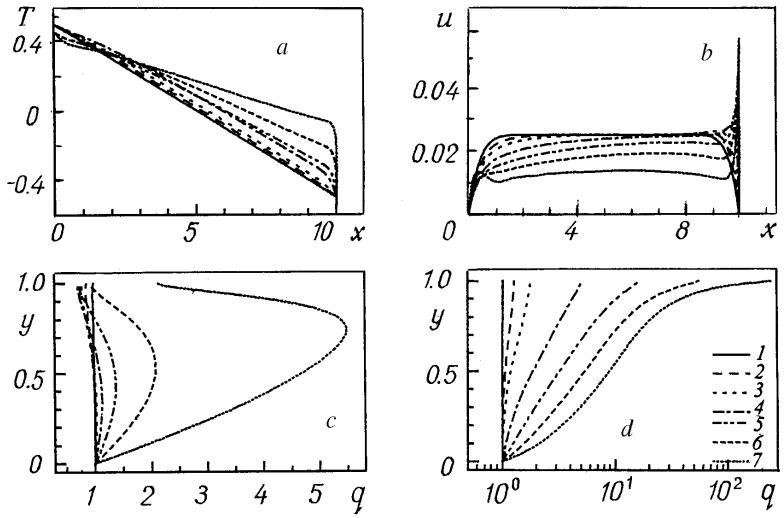

Fig. 2. Evolution of local characteristics with increase in Ma: [1) Ma = 10; 2) 100; 3) 200; 4) 500; 5) 1000; 6) 2000; 7) 1500]: a) temperature distributions along the free surface; b) distributions of the longitudinal component of velocity along the free surface; dimensionless heat-transfer coefficient; c) near the hot wall; d) near the cold wall.

from the heat-emitting and heat-receiving portions of the bottom. The overall heat flux from the heat-emitting surfaces $Q_{13} = Q_1 + Q_3 = Q_2 + Q_4 = Q_{24}$ is equal to that received by the cold walls. The contribution of the conductive Q_λ and convective Q_{con} mechanisms of heat transfer was investigated run on (Fig. 3b) in the entire range of Ma: $Q_\Sigma = Q_\lambda + Q_{con}$. The changes in the distributions over the flow section ($x = 5$) of the longitudinal heat-conducting (determined by the longitudinal component of the temperature gradient $-T_x$) and convective uT heat fluxes with increase in Ma are shown in Fig. 3c, d; the integrals of these profiles Q_λ and Q_{con_1} are given in Fig. 3b. Figure 3 demonstrates the integral heat-conducting $Q_\lambda = -\int_0^1 T_x(5, y)dy$ and convective $Q_{con} = \int_0^1 uTdy$ heat fluxes (in the section $x = 5$) in comparison with the integral heat flux on the walls of the cavity $Q_{24} = -\left[\int_0^1 T_x(10, y)dy + \int_{x^*}^{10} T_y(x, 0)dx\right] = \left[\int_0^1 T_x(0, y)dy + \int_0^{x^*} T_y(x, 0)dx\right]$ on the cold end face for different values of Ma. Here x^* is the coordinate of the inversion point of the sign of the local heat flux $q(x)$ on the lower boundary: $q(x^*) = 0$. It is seen from Fig. 3 that the relative contribution of the convective heat flux becomes equal to the heat-conducting one at Ma = 400. Thereafter, as Ma increases, the relative contribution of heat conduction slowly decreases and that of the convective heat flux increases.

The same trend is observed in all of the regimes of thermal gravitational convection, for example, in the case of a rigid adiabatic upper boundary [3] heat conduction remains the main mechanism of heat transfer up to Ra = 4000. Here, up to Ra = 100 the isotherms are strictly vertical, the temperature distribution along the x axis in different sections y_j merges into one straight line: $T(x, y_j) = 0.5 - x/A$. When Ra = 1000, the isotherms become slightly deformed. For Ra = 5000 the effect of convective motion on the shape of the isotherms becomes substantial and the longitudinal temperature profiles separate, that is, the earlier absent

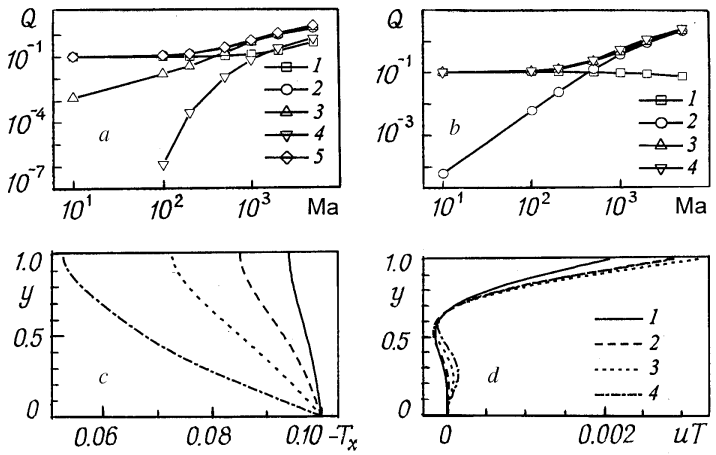

Fig. 3. Dependences of heat fluxes on Ma: a) dependences of the integral heat transfer on rigid walls [1) heat flux on a vertical hot wall; 2) on a vertical cold wall; 3 and 4) heat fluxes of heat-emitting and heat-receiving portions of the bottom, respectively; 5) total heat flux from heat-emitting surfaces equal to that received by the cold walls]; b) contribution of conductive (1) and convective (2) mechanisms of heat transfer, heat flux of heat-emitting portion (3) and total contribution of conductive and convective mechanisms of heat transfer (4); c, d) distribution, over the flow section (x = 5), of the longitudinal heat-conducting heat flux and longitudinal normalized convective heat flux [1) Ma = 500; 2) 1000; 3) 2000; 4) 5000].

stable lamination of liquid by temperature (and correspondingly by density) appears in the central portion of the cavity. In the regime of Ra = 10,000, there is already a noticeable stratification of liquid by temperature. A small portion of the unstably stratified boundary layer on the lower boundary appears. As Ra increases, the size of this portion and the value of the unstable temperature gradient increase. In the regime of Ra = 10^6, the isotherms in the core of the liquid layer are orientated almost horizontally. Thus, in the region of $y \geq 0.3$ the increase in Ra is accompanied by the formation of a nearly isothermal core, whereas in the lower region of $y < 0.3$ an unstably stratified boundary layer is formed. The scenario of this rearrangement of the temperature field agrees perfectly with experimental observations: the results of calculations coincide qualitatively and quantitatively with the results of measurements of temperature distributions in the vertical direction in different sections in the liquid layer bounded from below by a heat-conducting wall with a linear longitudinal distribution of temperature. Thereafter, in the experiment one observes (with increase in Ra) instability in the form of longitudinally oriented vortices, i.e., the flow becomes essentially three-dimensional.

The above-noted trends correlate with the dependences of integral heat fluxes on Ra and Ma numbers. Data similar to those presented in Fig. 3 allow one to determine exactly, for all the regimes, the limit of the existence of the heat-conduction regime: these are the values of Ra and Ma at which the intersection of the Q_λ and Q_{con} curves is observed. The isotherms near the cold wall were obtained for all of the regimes listed; they make it possible to predict the curvature of the crystallization front. Figure 4 presents some of the results of calculations of local characteristics in the regime of thermal gravitational-capillary convection in a system with linear distribution of T on the bottom: a and b represent the distributions of temperature and normalized velocity on a free surface; c shows the profiles of $u(y)$ in the central section $x = L/2$; d gives the distributions of the local coefficient of heat transfer on the cold wall. Here Ma is fixed, and the change in the characteristics with increase in Ra is shown. When Ra = $5 \cdot 10^3$, the effect of the buoyancy forces is barely perceptible. Everything is determined by thermocapillary convection. As Ra increases in the range of two

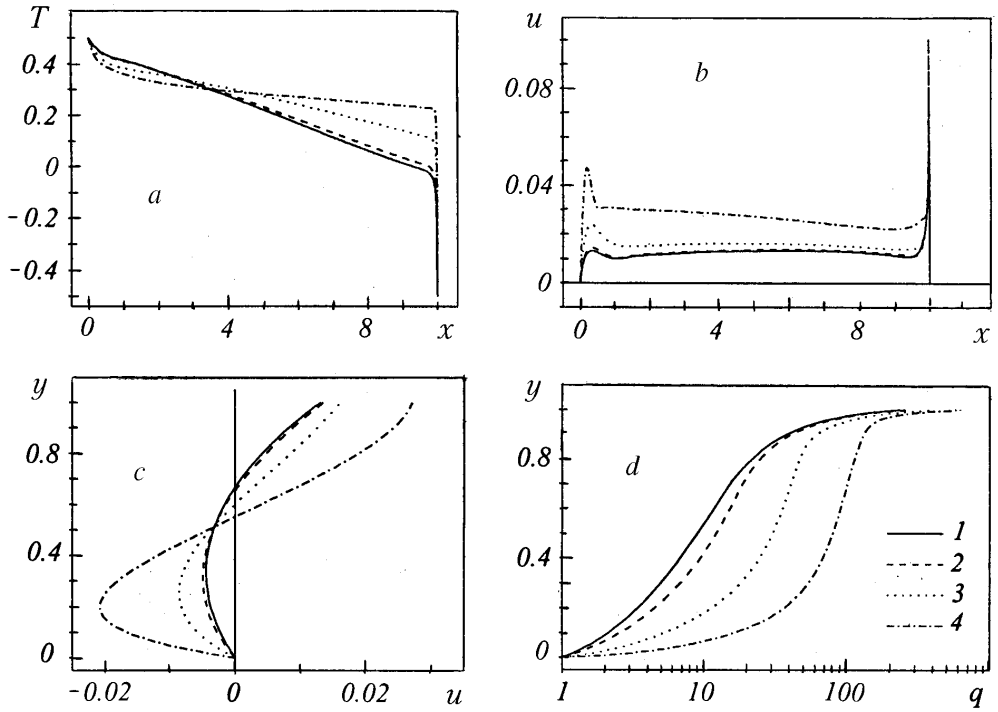

Fig. 4. Dependences of the local characteristics on Ra in the regime of thermal gravitational-capillary convection at Ma = 5000 [1) Ra = 100; 2) 5000; 3) 50,000; 4) 500,000]: a, b) distributions of T and u along the free surface; c) profiles of $u(y)$ in the central section x = 5; d) distributions of the local coefficient of heat transfer on the cold wall.

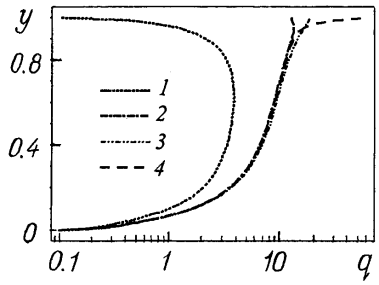

Fig. 5. Dependence of the local heat flux on the cold wall on the boundary conditions (Ra = 500,000; Ma = 5000): 1) a rigid upper boundary with a linear distribution of T; 2) rigid adiabatic; 3) free without friction; 4) free.

orders of magnitude of it, there occurs a transition to the regime of thermogravitational convection, against the background of which the thermocapillary effect is felt only near the cold wall. In the range $9.5 \le x \le 10$, the gradient of T is increased sharply, and on its background a local burst of the longitudinal velocity component is observed (the sharp maximum in Fig. 4b). In the zone of incidence onto the cold wall, the heat flux has a sharp local maximum. Such a maximum is absent in the regime of thermogravitational convection. In the regime of thermal gravitational-capillary convection, at any values of Ra the influence of the thermocapillary effect shows itself in the velocity gradient near the free surface being not equal to zero.

Figure 5 demonstrates the distributions of local heat fluxes on the cold wall at different boundary conditions for fixed values of Ra and Ma. Here, curve 1 corresponds to the case of a rigid upper boundary with a linear distribution of T; 2 to a rigid adiabatic boundary; 3 to a free, without friction, boundary; 4 to a

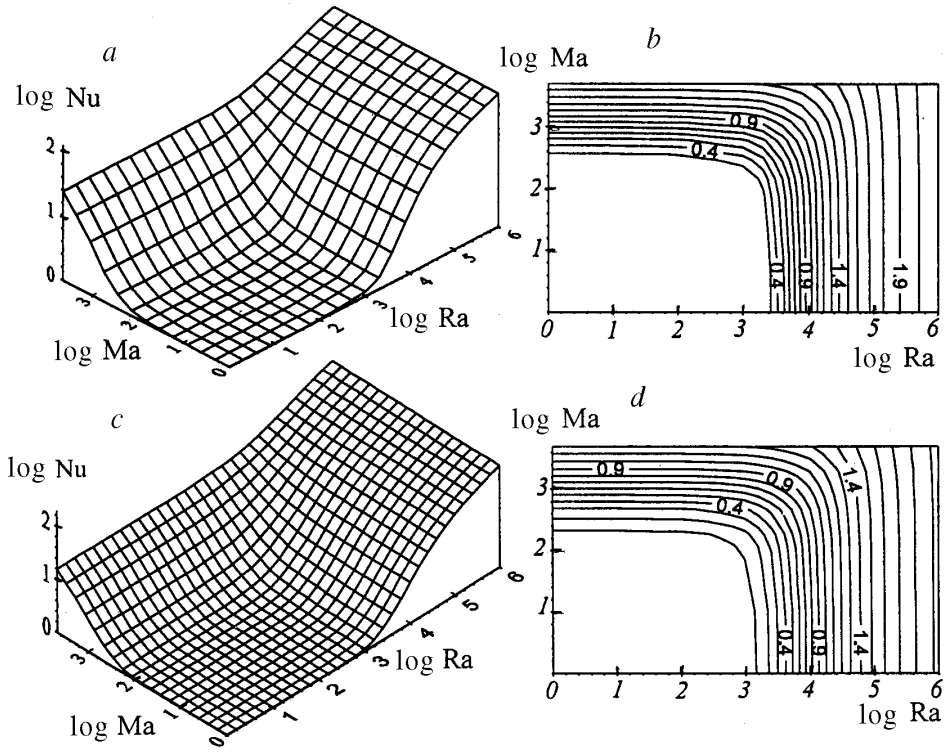

Fig. 6. Dependence of the dimensionless integral coefficient of heat transfer on Ra and Ma.

free one with Ma = 5000. The superposition of the gravitational and capillary effects is accompanied by a sharp burst of the heat flux in the region of contact of the free surface of the liquid with the cold wall.

The results of calculations of the integral coefficients of heat transfer in the regimes of thermal gravitational-capillary convection with linear distribution of T on the bottom are systematized in Fig. 6a, b and on an adiabatic bottom in Fig. 6c, d. The results are presented in the form of the surface of Nu (Ra, Ma) and in the form of the isolines log Nu on the plane {Ra, Ma}. In addition to the actual data on the values of Nu, it is very well seen here when (at what Ma) and to which extent, at a given value of Ra, the influence of the thermocapillary effect is felt against the background of thermogravitational convection and vice versa. Especially pronounced are the regions of the dominating influence of buoyancy forces against the background of thermocapillary convection or of the thermocapillary effect against the background of thermogravitational convection depending on the starting regime. From the comparison of the data given, it is seen that on the qualitative level the laws governing the mutual effect of the analyzed mechanisms of generation of flow depend weakly on the type of condition on the bottom of the cavity, but the absolute values of Nu depend greatly on them.

This work was carried out with financial support from the Russian Foundation for Basic Research (project code 99-01-00544) and Integration Projects of the Siberian Branch of the Russian Academy of Sciences Nos. 2000-49 and 2000-55.

NOTATION

A, ratio of the sides of the cavity; a, thermal diffusivity; H, height of the layer of liquid; L, length of the layer of liquid; Ma, Marangoni number, $\mathrm{Ma} = \Delta T \sigma_T H^2/\mu a L$; Nu, Nusselt number; Pr, Prandtl number, $\mathrm{Pr} = \nu/a$; $q(x)$, local heat flux on the bottom; $q(y)$, local heat flux on the vertical wall; Q, heat flux; Ra, Rayleigh number, $\mathrm{Ra} = \beta g \Delta T H^4/\nu a L$; T, dimensionless temperature; $T_x = \partial T/\partial x$, longitudinal component of

temperature gradient; $T_y = \partial T/\partial y$, transverse component of temperature gradient; $\{u, v\}$, dimensionless velocity vector; x, y, dimensionless coordinates; x_i, y_j, vertical and horizontal sections of the cavity, respectively; x^*, coordinate of the point of sign inversion; β, coefficient of volumetric expansion; ΔT, temperature difference between vertical walls; λ, thermal conductivity; μ, coefficient of dynamic viscosity; ν, coefficient of kinematic viscosity; $\sigma_T = -(\partial\sigma/\partial T)$, temperature coefficient of surface tension; ω, velocity curl; ψ, stream function. Subscripts: 1, vertical hot wall; 2, vertical cold wall; 3, heat-emitting portion of the bottom; 4, heat-receiving portion of the bottom; con, convective; λ, conducting; Σ, overall.

REFERENCES

1. V. S. Berdnikov and A. G. Zabrodin, in: *Thermophysical Processes in Crystallization of Substances*, Collection of Sci. Papers [in Russian], Novosibirsk (1987), pp. 67–99.
2. V. S. Berdnikov and A. G. Zabrodin, and V. A. Markov, in: *Hydromechanics and Transport Processes under Zero-Gravity* [in Russian], Sverdlovsk (1983), pp. 135–151.
3. V. S. Berdnikov and V. A. Gaponov, in: *Proc. 2nd Russ. Symp. "Processes of Heat and Mass Transfer and Growth of Monocrystals and Thin Film Structures"* [in Russian], Obninsk (1998), pp. 35–46.
4. R. V. Birikh, *Prikl. Mekh. Tekh. Fiz.*, No. 3, 69–72 (1966).
5. A. I. Tolstykh, *Compact Difference Schemes and Their Use in Aerodynamic Problems* [in Russian], Moscow (1990).
6. V. A. Gaponov, *Compact Difference Approximations of the Higher Order of Accuracy in the Problems of Computational Hydrodynamics*, Preprint No. 272-94 of the Institute of Thermophysics of the Russian Academy of Sciences [in Russian], Novosibirsk (1994).
7. V. A. Gaponov, in: *Proc. III Minsk Int. Forum "Heat and Mass Transfer MIF–96"* [in Russian], Vol. 1, Pt. 1, May 20–24, 1996, Minsk (1996), pp. 187–191.
8. V. I. Polezhaev, M. S. Bello, N. A. Verezub, et al., *Convective Processes under Zero-Gravity* [in Russian], Moscow (1991).